Journal of The Electrochemical Society, **158** (3) H338-H342 (2011)
0013-4651/2011/158(3)/H338/5/$28.00 © The Electrochemical Society

Effect of Annealing on the Microstructure and Electrical Property of RuN Thin Films

Chia-Yang Wu,[a] Wen-Hsi Lee,[a] Shih-Chieh Chang,[b] Yi-Lung Cheng,[c] and Ying-Lang Wang[b,z]

[a]*Department of Electrical Engineering, National Cheng Kung University, Tainan 701, Taiwan*
[b]*Institute of Lighting and Energy Photonics, National Chiao Tung University, Hsinchu 30050, Taiwan*
[c]*Department of Electrical Engineering, National Chi-Nan University, Nan-Tou, Taiwan*

Ruthenium (Ru) and ruthenium nitride (RuN) thin films have been investigated as candidates for barrier layers in copper (Cu) damascene processes. In order to study the thermal stability of the Ru and RuN films, the as-deposited films were annealed by rapid thermal annealing (RTA), and the film resistance was real-time measured by a four-point probe, which was embedded in the RTA tool. The X-ray diffraction data show that the grain size of Ru decreased with the increase of the nitrogen (N) content. The Ru phases gradually changed to the RuN phases, and the resistivity of the RuN films decreased with annealing time due to nitrogen effusion. Discontinuous RuN films were found when the annealing temperature was higher than 800°C and then caused a poor Cu diffusion barrier property. We also demonstrated that the Cu film could be directly electroplated on the RuN films with adequate adhesion.
 [DOI: 10.1149/1.3537825]

Manuscript submitted June 21, 2010; revised manuscript received November 22, 2010. Published January 25, 2011.

As the minimum feature size of microelectronic devices shrinks down to 32 nm and beyond, an increase in the resistivity of metal lines with feature shrinkage will be one of the semiconductor manufacturing challenges. In recent years, ruthenium (Ru) metal has been investigated as a barrier material for copper (Cu) metallization because (i) it facilitates direct electroplating of Cu without a seed layer; (ii) its adhesion to Cu is good even in the absence of a Cu seed layer; and (iii) its solubility in Cu is low, and thus its impurity effect on Cu resistivity will be minimal.[1-17] However, for pure Ru, it has been found that its barrier property for Cu diffusion is worse than that of tantalum and tantalum nitride (Ta/TaN) and Cu diffusion occurs after annealing at 450°C for 10 min in a Cu/Ru/Si structure.[1-4] Therefore, how to modify the Ru metal as a Cu plateable diffusion barrier layer is very important for Ru to replace Ta/TaN. Several reports found that the ruthenium nitride (RuN) barrier has a better thermal stability than that of the pure Ru.[5-8] Damayanti et al.[9] reported that these advantages can be attributed to the dissolved nitrogen (N) atoms in the amorphous films and the N atoms stuffed in the grain boundaries in the crystalline films, and the same report also clarified the peak of RuN phase on the X-ray diffraction (XRD) spectra.[9] Ogawa et al.[10] reported that the N atmospheres would only change the Ru into the amorphous type. In the same article, the stacked barrier structure (amorphous Ru/polycrystalline Ru) was proposed as a highly reliable barrier metal structure. In this study, we prepared RuN films with various N contents to investigate their barrier property and thermal stability. Furthermore, the phase transformation, the agglomeration behavior, the antidiffusion property, and the behavior of copper electroplating on various RuN films were studied by in situ sheet resistance (Rs) measurement, XRD, atomic force microscopy (AFM), scanning electron microscope (SEM), and X-ray photoelectron spectroscopy (XPS). Consequently, we may determine N content of the RuN films to optimize the barrier properties.

Experimental

A p-Si (111) wafer was chosen as the substrate for this study. The Ru layer (99.99% purity) was sputtered onto Si wafers at room temperature in a direct-current magnetron-sputtering machine. The base pressure and working pressure were controlled at 10^{-6} Torr and ~5 mTorr, respectively. Before sputtering, the sample was degassed at 300°C for 60 s. Deposition was carried out in nitrogen (N_2) and argon (Ar) atmosphere with different N_2 flow rates. The thickness of the Ru and RuN films was controlled at 20 nm, and then a 50-nm thick Cu (99.99% purity) layer was subsequently sputtered onto the samples at room temperature with a 5 mTorr working pressure.

Rapid thermal annealing (RTA) was applied to anneal the RuN/Si and Cu/RuN/Si for 5 min and 1 h, respectively. The annealing temperature was chosen between 100 and 800°C in N_2 and hydrogen (H_2) atmospheres. The texture was analyzed by XRD using a Bruker D8 SSS multipurpose thin-film X-ray diffractometer with 1.542 Å (Cu Kα) incident rays. The electron binding energy of Ru and the stoichiometric composition of the RuN films were measured by XPS. The films thickness and cross-sectional images were examined with HITACHI S-4800 SEM, while the surface roughness was measured using a NT-MDT P47E10 P7LS AFM. The sheet resistance was measured with a 280SI four-point probe.

A high-purity Cu sulfate ($CuSO_4 \cdot 5H_2O$, Aldrich) was dissolved in deionized water and sulfuric acid (H_2SO_4, Mallinckrodt) to make electrolytes for Cu electroplating. The electrochemical experiments were performed using an Autolab PGSTA302N. A conventional three-electrode cell with a Pt sheet as the counter electrode and Ag/AgCl (3 M KCl) as the reference electrode was employed. After Cu electroplating, 3M Scotch packing tapes were used to roughly check the adhesion between the Cu films and the Ru or RuN films.[2-4,15]

Results and Discussion

RuN/Si structure.— The different RuN samples were prepared with six different N_2 flow ratios (N_2/N_2 + Ar) that were from 0 to 56%. The resistivity and deposition rate of the Ru and RuN films are shown in Fig. 1a, which reveals that the film resistivity increased and the deposition rate decreased with the rise in the N_2 flow ratio. In this study, the resistivity of the RuN films was smaller than 80 μΩ cm, which was smaller than 150–200 μΩ cm of typical TaN films. The more N_2 gas in the reaction, the more Ru-N compounds were formed on the Ru target, resulting in a higher target resistance. The poison effect reduced the efficiency of the plasma bombardment to target and decreased the deposition rate of the RuN films. The XRD spectra of the RuN films with various N contents are shown in Fig. 1b. When the N_2 flow ratio was 0%, the prominent hexagonal peaks of Ru(100), Ru(002), and Ru(101) were found at 2θ = 38.38, 42.15, and 44.00°, respectively [Joint Committee for Powder Diffraction Standards (JCPDS) Card no. 06-0663]. When the N_2 flow ratio increased to 20%, the intensity of the Ru peaks declined while a new peak "face-centered cubic (fcc) RuN(200), 2θ = 40.5°" appeared.[11] When the N_2 flow ratio reached 33%, the RuN(200) peak became sharper but the Ru peaks, in contrast, almost disappeared. When the N_2 flow ratio reached 50%, only the RuN(200) peak remained.

[z] E-mail: ylwang@tsmc.com

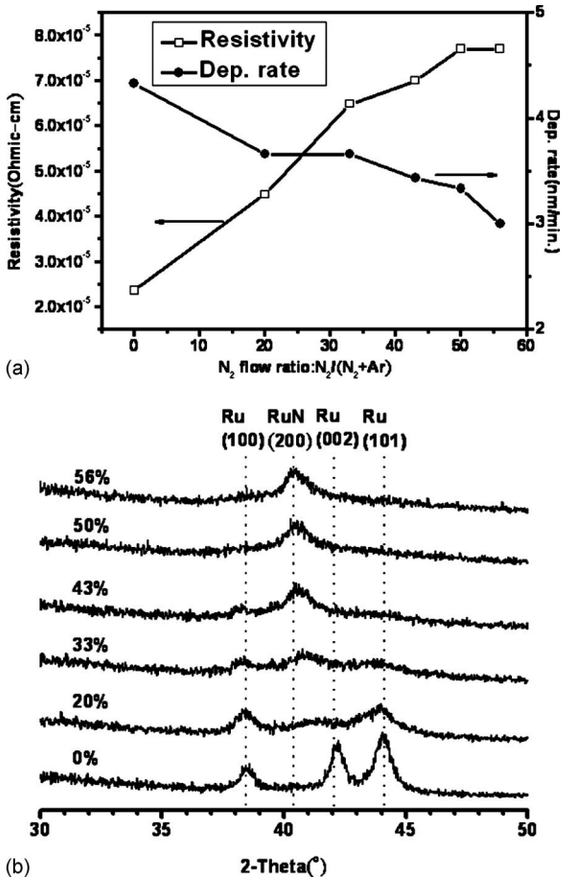

Figure 1. (a) Resistivity and deposition rate of the as-deposited RuN films. (b) XRD spectra of the as-deposited RuN/Si substrates with different N_2 flow ratios.

We also proved the existence of the RuN phases according to the result of XPS. Figure 2 shows that the binding energy of Ru peaks ($3d_{3/2}$: 284.2 eV, $3d_{5/2}$: 280.0 eV) was split and a part of them shifted slightly to a higher value. This phenomenon was due to the fact that the Ru atoms were in different valence states, inducing the chemical shift. The stoichiometric composition of the RuN films was also measured by XPS, as shown in Table I. It is obvious that

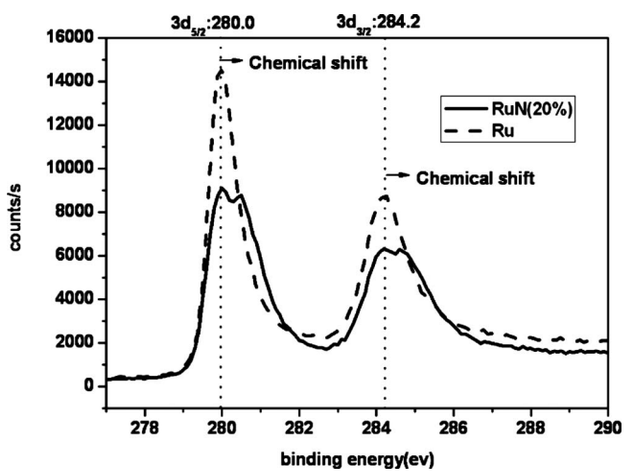

Figure 2. XPS spectra of the as-deposited pure Ru and RuN films.

Table I. Atomic ratio of Ru and RuN films.

Sputtering nitrogen ratio (N_2/N_2 + Ar) (%)	Ru atomic ratio (%)	N atomic ratio (%)
0	99.6	0.4
20	93.3	6.7
33	91.0	9.0
43	86.5	13.5
50	77.6	22.4
56	70.0	30.0

the N content of the RuN films increased with the rise in the N_2 flow ratio. The microstructures of the RuN films were examined by SEM. Figure 3a reveals that pure Ru has a column structure that has the paths for Cu diffusion during the annealing process. When the nitrogen mixes in, the column size decreases and the phase transforms into RuN, as shown in Fig. 3b. In addition, the grain size of Ru and RuN could be determined by Scherrer's formula. Applying the XRD result of Fig. 1b into the formula, we derived that the grain sizes of the Ru and RuN (20%) films were 12.73 and 5.85nm, respectively. Even though there are more grain boundaries in the RuN films than the Ru film, the grain boundaries in the RuN films do not extend from top to bottom, which could not provide direct diffusion paths for Cu. In contrast, the grain boundaries in the Ru films could provide direct diffusion paths for Cu. As mentioned earlier, we consider that the RuN film with proper N content had a better antidiffuse ability than the pure Ru film.

Figure 4 shows that the resistivity of all RuN samples decreased after annealing. The resistivity of the high N-content samples (43, 50, and 56%) decreased rapidly when the annealing temperature was above 100°C. On the other hand, the resistivity of the low N-content samples (20 and 33%) decreased when the temperature was above 200°C. The N effusion rate was higher in the high N-content

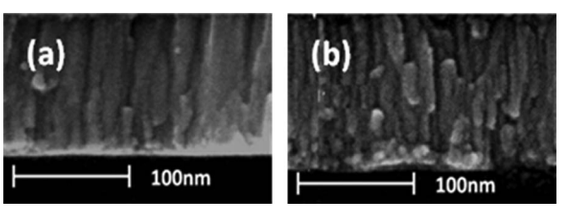

Figure 3. Microstructures of the as-deposited RuN/Si substrates with different N_2 flow ratios: (a) 0 and (b) 20%.

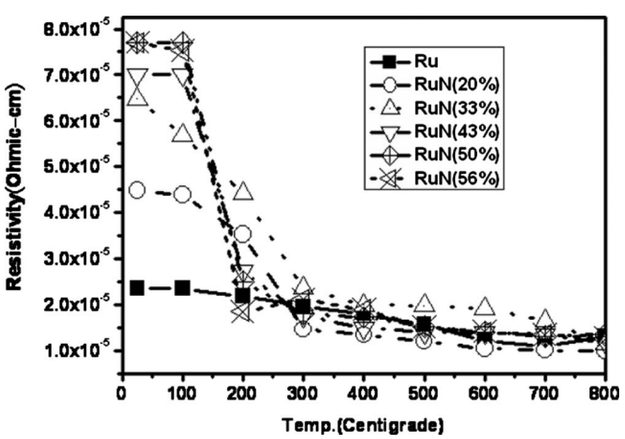

Figure 4. Resistivity of the RuN samples after annealing from 100 to 800°C.

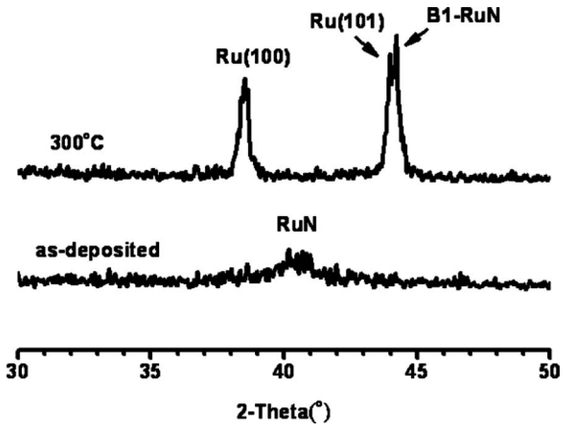

Figure 5. XRD results of the as-deposited RuN (56%) sample and the sample annealed at 300°C.

samples because more nitrogen atoms did not bond with Ru atoms in the high N-content samples, whereas the nitrogen atoms in the low N-content samples almost bonded with Ru atoms.

Annealing also provides sufficient energy to decompose the unstable Ru-N bonding and to transform the RuN film into the hexagonal crystals. The XRD results of Fig. 5 show that the lower one

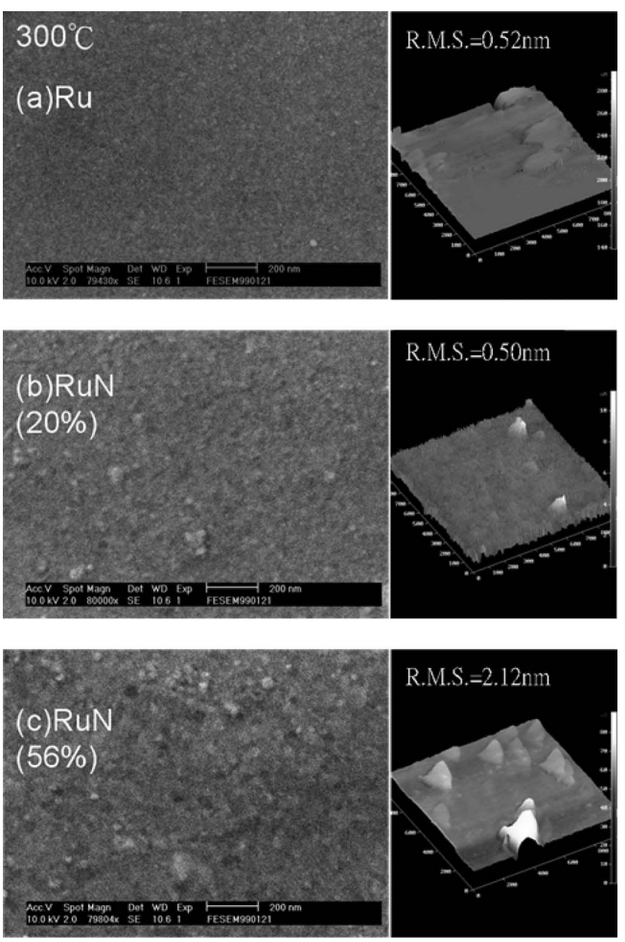

Figure 6. SEM images and AFM micrographs of (a) Ru/Si; (b) RuN (20%)/Si; and (c) RuN (56%)/Si after annealing at 300°C for 5 min.

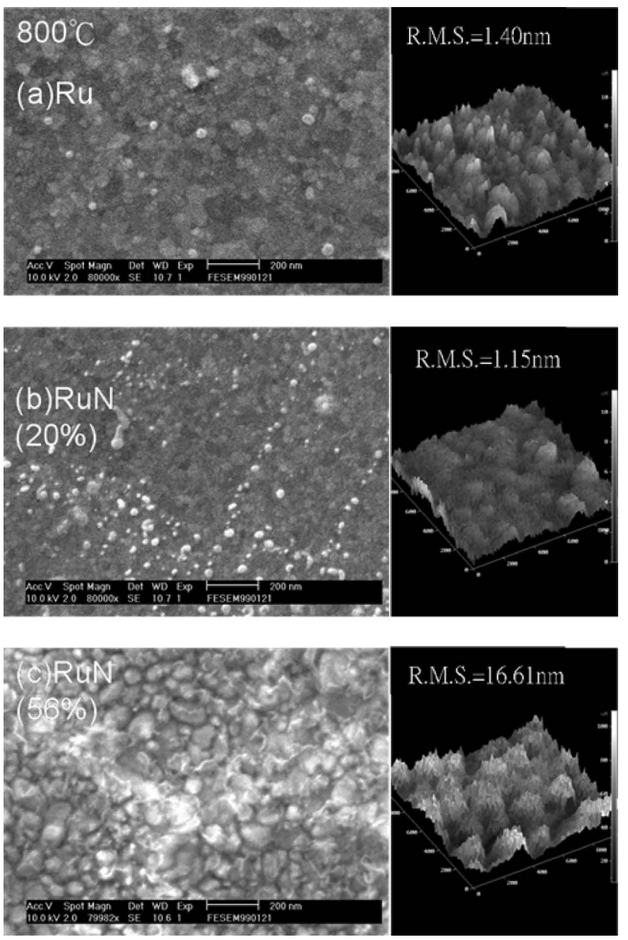

Figure 7. SEM images and AFM micrographs of (a) Ru/Si; (b) RuN (20%)/Si; and (c) RuN (56%)/Si after annealing at 800°C for 5 min.

was the as-deposited RuN (56%) sample and the upper one was the sample annealed at 300°C. Ihara et al.[11] reported that there were a large amount of nitrogen vacancies in the RuN films after annealing. Not only hexagonal structures but also fcc ones were formed in the RuN films, meaning that there were fewer paths for Cu diffusion,

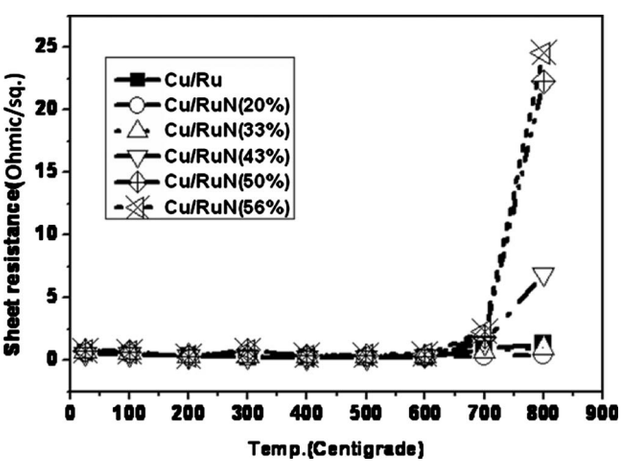

Figure 8. Resistivity vs annealing temperature (from 100 to 800°C) of Cu/RuN/Si structures.

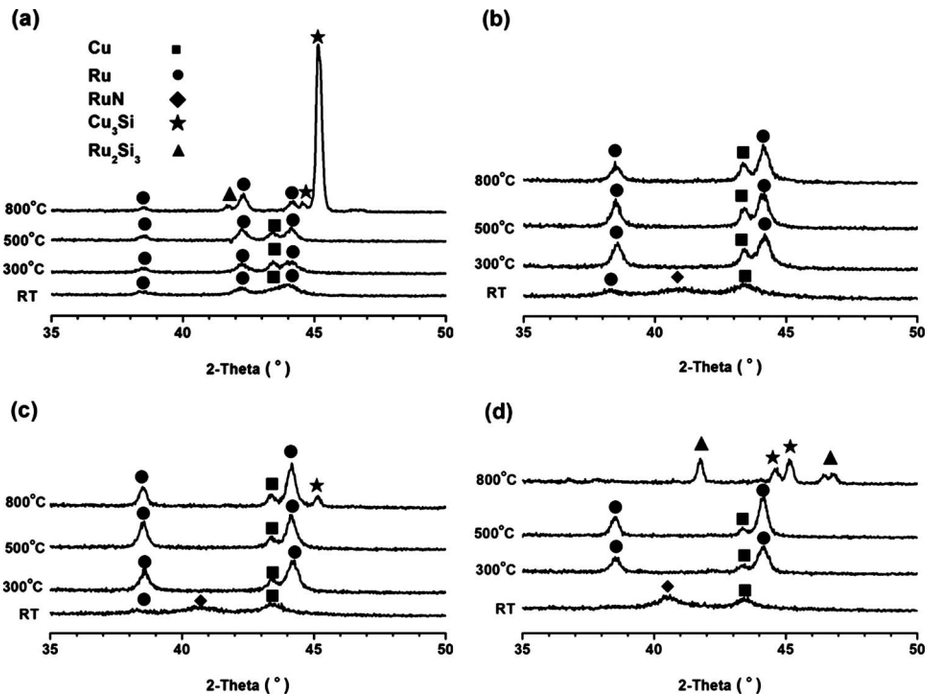

Figure 9. XRD textures of different RuN films after annealing from 300 to 800°C for 1 h: (a) Cu/Ru/Si; (b) Cu/RuN (20%)/Si; (c) Cu/RuN (33%)/Si; and (d) Cu/RuN (56%)/Si.

and this is why the RuN barrier had a better antidiffusion property even when the phase was changed after annealing. Furthermore, N atoms effused from the RuN films after annealing, and this may induce some unfavorable phenomenon on the surface of the RuN films. We can see from the SEM images shown in Figs. 6 and 7 that pure Ru and the low N-content (20%) RuN films had smoother surfaces whereas the high N-content (56%) RuN films became rougher after 300 or 800°C annealing. There were many bulges on the surface when the annealing temperature was set at 300°C. It was suspected that the worse thermal stability of the high N-content RuN films was due to a large amount of nitrogen vacancies after nitrogen effusion. As mentioned above, annealing provides sufficient energy to transform the RuN films into hexagonal crystals, and defects were formed by nitrogen effusion at the same time. The effused N content could make some vacancies in the film, resulting in a rough surface after annealing. The AFM micrographs of Figs. 6 and 7 could support the model.

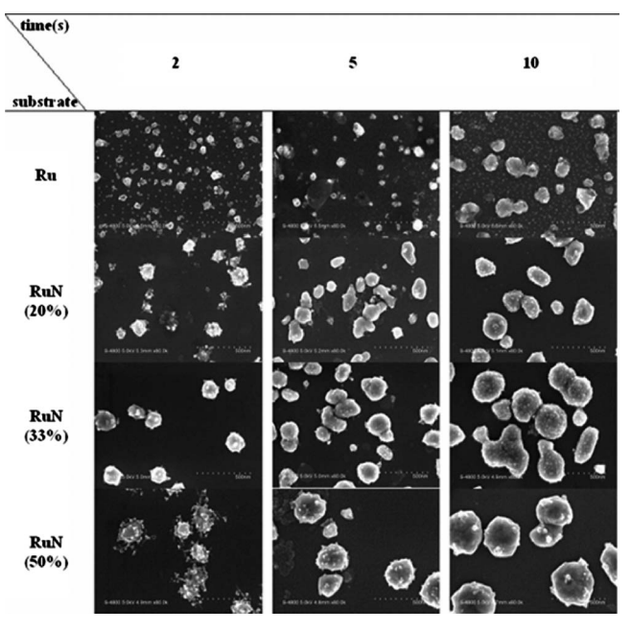

Figure 10. SEM images of electroplated Cu clusters on different RuN substrates with various plating times.

Cu/RuN/Si structure.— We deposited a 50-nm thick Cu layer onto the RuN films to check their barrier properties for Cu diffusion. Figure 8 shows that the resistivity of the high N-content (43, 50, and 56%) RuN films rose steeply when the annealing temperature was above 700°C. In contrast, the resistivity increased slightly in the pure Ru and low N-content RuN films. It was suggested that the increase in the film resistivity was due to the formation of Cu silicide. In particular, the resistivity of the RuN (20%) sample only rose slightly even when the annealing temperature was higher than 800°C. In this case, we want to clarify the relationships between the crystalline structure and the diffusion behavior. Figure 9 shows the XRD results of the RuN films with different conditions after the annealing process. For the Cu/Ru/Si sample, both the Ru_2Si_3 peak and the striking Cu_3Si peak formed, and none of the Cu phase remained when the annealing temperature rose to 800°C. The presence of Cu_3Si demonstrated that Cu diffused into Si through the barrier layer.[5,7,12-15] A similar case is that there were both Ru_2Si_3 and Cu_3Si peaks in the Cu/RuN (56%)/Si sample. Overall, the RuN (20%) film had the best barrier property among the samples. There was no Cu silicide or Ru silicide remaining in the Cu/RuN (20%)/Si sample even after 800°C annealing. When the N_2 flow ratio increased to 33%, the Cu_3Si phase appeared, and there were still some Ru and Cu phases remaining after annealing. Ru_2Si_3 is currently an imperfect product in the metallization process, which can adversely affect device quality. However, this study found that the optimization of nitrogen content in the RuN films reduced not only Cu diffusion but also the formation of Ru_2Si_3.

Electrodeposition of Cu on RuN.— Figure 10 shows the SEM top-view images of the nucleation behavior of Cu electroplating on different RuN substrates and plating times. It was found that small Cu clusters were reduced on the substrate at first and then gradually became larger with the plating time from 2 to 10 s. The Cu nucleation rate decreased with the rise of the N content; however, larger

Cu clusters were formed on the N-rich RuN substrates at the plating time of 10 s. In this study, both the Ru and RuN films were demonstrated to be a plateable layer for Cu electroplating. As the minimum feature size of microelectronic devices shrinks, the overall barrier and seed thickness were critical for the gap-filling process window of subsequent Cu electroplating process. The plateable RuN film could act as both a barrier and seed layers to reduce overall thickness as compared with the current Ta/TaN barrier and Cu seed layers. After Cu electroplating, we then used 3M Scotch packing tape to test the adhesion between the Cu and Ru/RuN substrates, and all of the samples remained intact after the test.

Conclusion

The RuN films deposited in the N_2 and Ar atmospheres were assessed as a good diffusion barrier for Cu. The resistivity of the RuN films decreased with increasing annealing temperature. However, the RuN films with a too high N content had a rougher surface and more vacancies after annealing due to more nitrogen effusion. The diffusion of Cu through the RuN film was slower as compared with the Ru film because the RuN films had a less direct diffusion path for Cu as compared with the Ru film. However, when the N content was too high, too many vacancies may be formed after annealing due to nitrogen effusion, resulting in a poor barrier property for Cu diffusion. In this study, the 20% N_2 flow ratio was the best condition for the RuN barrier properties. We also demonstrated that the Cu film could be directly electroplated on the RuN films with adequate adhesion.

Acknowledgments

The authors thank National Cheng Kung University, Tainan, Taiwan, for its technical support.

References

1. M. Damayanti, T. Sritharan, Z. H. Gan, S. G. Mhaisalkar, N. Jiang, and L. Chanb, *J. Electrochem. Soc.*, **153**, J41 (2006).
2. T. P. Moffat, M. Walker, P. J. Chen, J. E. Bonevich, W. F. Egelhoff, L. Richter, C. Witt, T. Aaltonen, M. Ritala, M. Leskelä, et al., *J. Electrochem. Soc.*, **153**, C37 (2006).
3. O. Chyan, T. N. Arunagiri, and T. Ponnuswamy, *J. Electrochem. Soc.*, **150**, C347 (2003).
4. R. Chan, T. N. Arunagiri, Y. Zhang, O. Chyan, R. M. Wallace, M. J. Kim, and T. Q. Hurdc, *Electrochem. Solid-State Lett.*, **7**, G154 (2004).
5. J. P. Chu, C. H. Lin, and V. S. John, *Appl. Phys. Lett.*, **91**, 132109 (2007).
6. M. Damayanti, T. Sritharan, S. G. Mhaisalkar, H. J. Engelmann, E. Zschech, A. V. Vairagar, and L. Chana, *Electrochem. Solid-State Lett.*, **10**, P15 (2007).
7. C. W. Chen, J. S. Chen, and J. S. Jeng, *J. Electrochem. Soc.*, **155**, H438 (2008).
8. M. Kawamura, K. Yagi, Y. Abe, and K. Sasaki, *Thin Solid Films*, **494**, 240 (2006).
9. M. Damayantia, T. Sritharan, S. G. Mhaisalkar, and Z. H. Gan, *Appl. Phys. Lett.*, **88**, 044101 (2006).
10. S. Ogawa, N. Tarumi, M. Abe, M. Shiohara, H. Imamura, and S. Kondo, in *Interconnect Technology Conference, IITC 2008. International*, p. 102 (2008).
11. H. Ihara, N. Terada, K. Senzaki, M. Hirabayashi, Y. Kimura, R. Uzuka, F. Kawashima, and M. Akimoto, *IEEE Trans. Magn.*, **23**, 1011 (1987).
12. J. J. Tan, X. P. Qu, Q. Xie, Y. Zhou, and G. P. Ru, *Thin Solid Films*, **504**, 231 (2006).
13. D. C. Perng, J. B. Yeh, and K. C. Hsu, *Appl. Surf. Sci.*, **254**, 6059 (2008).
14. H. Kim, T. Koseki, T. Ohba, T. Ohta, Y. Kojima, H. Sato, and Y. Shimogakia, *J. Electrochem. Soc.*, **152**, G594 (2005).
15. S. H. Kwon, O. K. Kwon, J. S. Min, and S. W. Kang, *J. Electrochem. Soc.*, **153**, G578 (2006).
16. M. Stavrev, D. Fischer, and F. Praessler, *J. Vac. Sci. Technol. A*, **17**, 993 (1999).
17. C. Ryu, A. L. S. Loke, T. Nogami, and S. S. Wong, *IEEE Int. Reliab. Phys. Symp. Proc.*, **1997**, 201.